DØnote 4561-Conf, v1.2

Search for Technicolor Particles ρ_T and ω_T in the Dielectron Channel with 200 pb^{-1} of Data with the DØ Detector

The DØ Collaboration

URL: http://www-d0.fnal.gov

(Dated: August 6, 2004)

We present preliminary results of searches for technirho (ρ_T), and techniomega (ω_T) particles, using the decay channels $\rho_T, \omega_T \to e^+e^-$. The search is based on 200 pb^{-1} of data collected in Run II of the Fermilab Tevatron. In the absence of a signal, we set 95% CL upper limits on the cross sections for the process $\rho_T, \omega_T \to e^+e^-$ as a function of the mass of the decaying particle. For certain model parameters, we exclude the existence of degenerate ρ_T and ω_T states with masses below 367 GeV. Limits obtained in this analysis are the most restrictive constraints on dilepton technicolor decays to date.

Preliminary Results for Summer 2004 Conferences

I. INTRODUCTION

Historically, the decay to lepton-antilepton pairs – in particular e^+e^- and $\mu^+\mu^-$ – has been an important discovery channel for new particles. The J/ψ, Υ, and Z have all been discovered in this way. Many extensions of the standard model predict the existence of particles that decay to lepton-antilepton pairs. Examples are heavy gauge bosons (Z') and technihadrons (ρ_T, ω_T).

The lepton-antilepton signature is a preferred channel for particle searches in strong interactions because of the relatively low backgrounds compared to hadronic decay channels. Electrons are relatively easy to trigger on and their momenta can be measured precisely. Thus particles that decay to e^+e^- can be identified as resonances in the dilepton mass spectrum.

We describe a search for techniparticle resonances in the e^+e^- mass spectrum from the data collected by DØ during Run II of the Fermilab Tevatron. This analysis is a straightforward extension of the searches for TeV^{-1} extra dimensions in the dielectron channel [1] and the search for the Z' [2].

The data, background, efficiencies, and systematic errors are the same as in the former analyses. The extraction of limits on the techniparticles is based solely on the dielectron mass spectrum, shown in Fig. 1. Since the fraction of instrumental background is similar in the two topologies studied, where both electrons are in the central calorimeter cryostat (CC-CC) or one electron is in the central cryostat and one is in the end-cap cryostat (CC-EC), for the purpose of this search we combine spectra for these two topologies rather than performing a more involved, Bayesian fit for each topology and then combining the results by combining the likelihoods.

The present analysis is based on a counting experiment in a window around the assumed technirho and techniomega masses, with the optimal width, which depends on the mass. The details of the method, all the systematics uncertainties, selection and cross section limits are the same as in the search for Z' [2], so they are repeated here only briefly.

II. THE TECHNICOLOR MODEL

Recent topcolor-assisted technicolor models with walking gauge coupling require many technihadron states. These models predict the existence of scalar mesons, the technipions ($\pi_T^\pm$ and π_T^0), and vector mesons (ρ_T and ω_T). These technihadron states are expected to be produced with substantial rates at the Tevatron [3]. The vector mesons decay to $\gamma\pi_T$, $W\pi_T$, $Z\pi_T$, or $f\overline{f}$. No large isospin violating technicolor interactions are needed to explain the mass difference between the top and bottom quarks. Therefore, the ρ_T and ω_T states can be (and are assumed to be) degenerate in mass. As shown in Ref. [4], most of the rate to dilepton final states originates from ω_T decays, so that our conclusions for the mass of the ω_T do not depend strongly on this assumption.

The values of $\sigma(\rho_T,\omega_T) \times B(\rho_T,\omega_T \to \ell\ell)$ depend on the following factors:

- mass of ρ_T (M_{ρ_T}) and ω_T (M_{ω_T})
- mass difference between the vector mesons (ρ_T, ω_T) and the technipions, which determines the spectrum of accessible decay channels.

In addition, the ω_T production cross section is sensitive to the charges of the technifermions. There two mass parameters in the model: M_A for axial-vector and M_V for vector couplings. Their values are expected to be comparable. The mass parameter M_V controls the rate for $\omega_T \to \gamma + \pi_T^0$. and is unknown *a priori*. Scaling from the decay $\omega \to \gamma + \pi^0$ the authors[4–6] suggest a value of several 100 GeV. We set $M_A = M_V$. For all other parameters, we use the default values quoted in Table 2 of Ref. [4, 6],

We use recently updated calculations of the cross sections for $p\overline{p} \to \rho_T \to \ell^+\ell^-$ and $p\overline{p} \to \omega_T \to \ell^+\ell^-$ [4, 5]. Previously published searches for technicolor particles [7] use older calculations. When comparing limits this must be taken into account. The predictions for the cross sections of the processes $p\overline{p} \to (\rho_T \text{ or } \omega_T) \to e^+e^-$ are plotted in Fig. 2. In this figure, the two sets of predictions shown differ in the assumed mass difference between the vector and scalar mesons. For a mass difference smaller than the mass of the W boson (e.g. 60 GeV), the decay $\rho_T \to W + \pi_T$ is forbidden and the branching ratio (shown as blue curves) to dielectrons is enhanced compared to the case of a mass difference of 100 GeV, for which the $W\pi_T$ mode is allowed (shown as magenta curves). The three curves for each set corresponds to values of M_V=500 GeV (uppermost), 200 GeV (middle) and 100 GeV (lowermost) respectively.

III. SEARCH FOR ρ_T, ω_T IN THE DIELECTRON CHANNEL

A. Data Selection

The data used for this analysis was selected using all the available recent data from DØ Run II, i.e. data taken between April 2002 and November 2003. All the data have been reconstructed with the DØ reconstruction program. These data correspond to the total intergrated luminosity of ≈ 200 pb^{-1} and have been collected via a suite of single EM and diEM triggers, which run unprescaled at all instantaneous luminosities. Given that the analysis is concerned only with high-p_T EM objects, the trigger is $99 \pm 1\%$ efficient for the signal.

We require two EM objects in the event, with the transverse energies above 25 GeV, which pass calorimeter energy isolation, EM energy fraction, and calorimeter shower shape cuts. At least one of the EM objects is required to have a matching track in the tracking detectors. Primary vertex in the event is defined via this track. We reject events that have more than two high-p_T EM objects. The EM clusters are restricted to good fiducial volume of the DØ EM calorimeter: $|\eta_d| < 1.1$ (CC) and $1.5 < |\eta_d| < 2.4$ (EC), where η_d is pseudorapidity, as measured w.r.t. the geometrical center of the DØ detector.

For the details of the preselection, see Ref. [8]. The overall efficiency of the event selection are as folows [1]:

$$\varepsilon_{\mathrm{CC-CC}} = 0.74 \pm 0.02; \quad (1)$$

$$\varepsilon_{\mathrm{CC-EC}} = 0.74 \pm 0.02; \quad (2)$$

The analysis sample consists of 14,195 events, corresponding to 8,246 CC-CC and 5,949 CC-EC combinations. The event selection flow is detailed in Table I.

TABLE I: Number of Data Events at Various Level of Event selection.

Cut	Number of events
Reconstructed Data	~700 million events
≥ 2 EM objects w/ $E_T > 20$ GeV and χ^2 cut	39,604
$E_T^{EM} > 25$ GeV, EMF cut, track match	15,602
At least one central EM object	14,195 = 8,246 CC-CC + 5,949 CC-EC

The integrated luminosity on this sample is known with 6.5% uncertainty (dominated by the uncertainty in the world average for the total inelastic cross section). In order to decrease the dependence on the luminosity measurement, we normalize all the cross sections to the NNLO Z production cross section, known well theoretically [9].

B. Event Yields and Backgrounds

The QCD background is estimated via the method of Ref. [1]. The Drell-Yan background is simulated with the parton-level Monte Carlo generator of Ref. [8], augmented with a parametric simulation of the DØ detector. The simulation takes into account detector acceptance, efficiencies, and resolution, initial state radiation, and the effect of different parton distributions. We used leading order CTEQ4LO [10] distributions to estimate the nominal prediction. The parameters of the detector model are tuned using the $Z(ee)$ data.

Since the parton-level generator involves only the $2 \to 2$ hard-scattering process, we model next-to-leading order (NLO) effects by adding a transverse momentum to the diEM system, based on the measured transverse momentum spectrum of the $Z(ee)$ events. Since the parton-level cross section is calculated at LO, we account for NLO effects in the SM background by scaling the cross sections by a constant K-factor of 1.3 [9].

The K-factor for Z/γ^* exchange tends to grow with mass [9]. Consequently, our assumption of a flat K-factor tends to underestimate the contribution from the SM (i.e., background) and thus is conservative in terms of sensitivity to the techniparticle production.

Since the direct diphoton production is at least an order of magnitude less than Drell-Yan production even at high masses, background from direct diphotons with photon conversions is negligible. All other physics backgrounds that result in dielectron final state are negligible.

The intrinsic width of the ρ_T and ω_T for the range of the parameters tested in this analysis is around half a GeV, and thus small compared to the dielectron mass resolution of the DØ calorimeter. This is similar to the case of the search for Z'; and therefore we use the same technique for optimizing the size of the counting window as is the search for the Z' [2].

TABLE II: Optimum window sizes and the results of the counting experiment in these windows.

ρ_T, ω_T Mass	Window	QCD bck.	DY bck.	Total bck.	Bck. Err	Data
160 GeV	150–170 GeV	42.1	43.4	85.5	8.6	77
180 GeV	170–190 GeV	24.1	25.1	49.2	4.9	48
200 GeV	190–210 GeV	13.3	15.6	28.9	2.9	23
220 GeV	200–240 GeV	12.5	17.7	30.2	3.0	18
240 GeV	220–260 GeV	7.32	12.0	19.4	1.9	13
260 GeV	240–280 GeV	4.25	8.40	12.6	1.3	8
280 GeV	260–300 GeV	2.66	5.96	8.61	0.86	5
300 GeV	270–330 GeV	2.59	6.23	8.82	0.88	4
320 GeV	290–350 GeV	1.67	4.60	6.26	0.63	3
340 GeV	310–370 GeV	1.03	3.42	4.44	0.44	2
360 GeV	330–390 GeV	0.65	2.57	3.21	0.32	2
380 GeV	350–410 GeV	0.31	1.95	2.26	0.23	3
400 GeV	380–430 GeV	0.21	1.49	1.71	0.17	2

TABLE III: Leading order production cross-section and acceptances for $\rho_T, \omega_T \to ee$ for a mass parameter $M_V = 100$ GeV and $M(\rho_T) - M(\pi_T) = 60$ GeV (from PYTHIA). Only statistical uncertainties are shown.

ρ_T, ω_T Mass	$\sigma(\rho_T, \omega_T) \times B(\rho_T, \omega_T \to ee)$	K-factor $(K(M))$	Acceptance CC-CC	Acceptance CC-EC	Acceptance Total
160	0.90 pb	1.30	0.234 ± 0.004	0.226 ± 0.004	0.460 ± 0.005
180	0.56 pb	1.30	0.249 ± 0.004	0.213 ± 0.004	0.463 ± 0.005
200	0.38 pb	1.30	0.264 ± 0.004	0.196 ± 0.004	0.460 ± 0.005
220	0.27 pb	1.30	0.332 ± 0.005	0.228 ± 0.004	0.560 ± 0.005
240	0.19 pb	1.30	0.345 ± 0.005	0.222 ± 0.004	0.567 ± 0.005
260	0.14 pb	1.30	0.354 ± 0.005	0.223 ± 0.004	0.577 ± 0.005
280	0.11 pb	1.30	0.357 ± 0.005	0.200 ± 0.004	0.557 ± 0.005
300	0.082 pb	1.30	0.385 ± 0.005	0.205 ± 0.004	0.590 ± 0.005
320	0.065 pb	1.30	0.407 ± 0.005	0.187 ± 0.004	0.594 ± 0.005
340	0.051 pb	1.30	0.409 ± 0.005	0.185 ± 0.004	0.594 ± 0.005
360	0.040 pb	1.30	0.415 ± 0.005	0.180 ± 0.004	0.595 ± 0.005
380	0.033 pb	1.30	0.415 ± 0.005	0.172 ± 0.004	0.587 ± 0.005
400	0.026 pb	1.30	0.428 ± 0.005	0.154 ± 0.004	0.581 ± 0.005

The results of the counting experiments in each mass window are summarized in Table II.

Since the data in each window are consistent with the expected background, we proceed with setting limits on the existence of the techniparticles ρ_T and ω_T.

C. Acceptance Calculation

The acceptance and cross-section for the production of ρ_T and ω_T was calculated using Pythia 6.220 [11] with CTEQ5L pdf's [12] and the DØ parametrized fast detector simulation for electron smearing based on the measured calorimeter resolution for electromagnetic objects. No geometrical fiducial cuts are applied. Masses from 200–400 GeV were generated with only the ρ_T and ω_T production turned on at the generator level and its decays to electron pairs. Simulated events were accepted if two electrons had $p_T > 25$ GeV/c at the generator level and were in the fiducial pseudorapidity range of $|\eta| < 1.1$ (CC) or $1.5 < |\eta| < 2.4$ (EC), with only CC-CC and CC-EC combinations being accepted. The invariant mass was calculated from the simulated electrons and the mass window cut of Table II was applied. Table III shows the generated cross-section for $\rho_T, \omega_T \to ee$ and the corresponding acceptances.

The statistical uncertainty is about 1% based on 10,000 event samples. A conservative overall 5% uncertainty is chosen to cover mass dependence of the pdf's.

The LO PYTHIA cross section for technirho and techniomega production is multiplied by the flat K-factor of 1.3. While no NLO calculations for techniparticle production exist yet, we assume the K-factor similar to that in the Drell-Yan or Z' production, as most of the NLO corrections come from the initial state radiation, which is similar in the case of DY and techniparticle production. The K-factor and the cross section are shown in Table III.

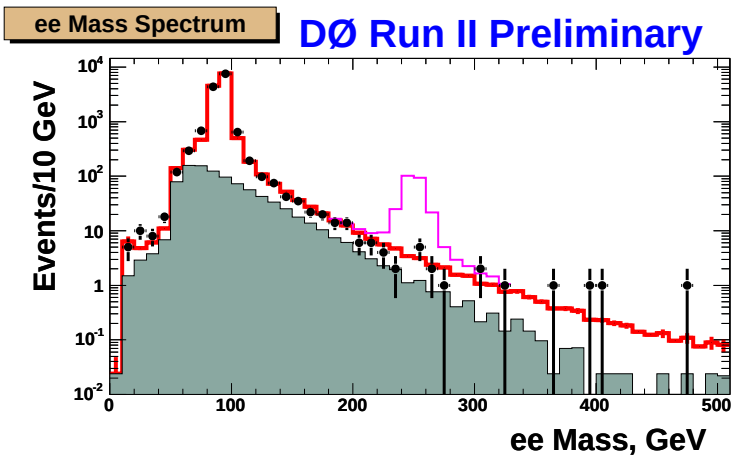

FIG. 1: Dielectron mass distribution. Points: data; shaded region: QCD background; open histogram: sum of the Drell-Yan and QCD background. Also shown: the ρ_T, ω_T signal for a mass of 250 GeV (magenta histogram). Signal cross section corresponds to $M_V = 100$ GeV, $M(\rho_T) - M(\pi_T) = 60$ GeV and was multiplied by a factor of ten.

D. Systematics

We consider various sources of systematic uncertainties for signal and background, which are documented in Table IV.

We use NNLO Z cross section in the e^+e^- channel of 252 ± 9 pb [9] to determine the integrated luminosity in our sample, thus effectively normalizing techniparticle production cross section to that of the Z.

The overall 9% signal cross section uncertainty includes E_T/η dependence of the efficiency of 7%, theoretical uncertainty on the NNLO Z cross section of 4%, and signal acceptance uncertainty of 5%. The central value of the integrated luminosity determined by this method corresponds to 181 pb^{-1}, in a good agreement with the 196 ± 13 pb^{-1} from the DØ luminosity measurement.

Source of signal systematics	Uncertainty
E_T and η dependence of the efficiency	7%
Signal acceptance uncertainty	5%
Z cross section uncertainty	4%
Total	9%
QCD background uncertainty	10%
DY background uncertainty	10%

TABLE IV: Sources of systematic uncertainties used in this analysis.

The QCD background uncertainty stems from the uncertainty on normalization at low masses, which is slightly less than 10%; the DY background uncertainty mainly stem from the fact that we conservatively use a flat K-factor for DY, which results in 10% uncertainty due to the mass-dependence of the K-factor.

E. Limits on the ρ_T and ω_T cross section and constraints on the Technicolor model

In order to set the limits on the $\rho_T, \omega_T \to e^+e^-$ cross section, we use counting experiment in each mass window. We measure the effective integrated luminosity in our sample based on the central value of the NNLO $Z(ee)$ cross section of 252 ± 9 pb [9].

A standard Bayesian limit-setting procedure [13] with the signal and background systematics discussed above is applied. The results are listed in Table V and shown in Fig. 2 as a function of the ρ_T, ω_T mass. Fig. 2 also shows the cross-sections predicted for various values of technicolor model parameter M_V and the mass difference $M(\rho_T) - M(\pi_T)$.

These limits can be translated into constraints on the masses of the techniparticles ρ_T, ω_T. The results are shown in Fig. 2. We find that we can rule out ρ_T and ω_T with masses below 367 GeV (355 GeV), if the mass difference between ρ_T and $\pi_T^{\pm}$ is smaller (larger) than the W mass, for the mass parameter M_v set at 500 GeV.

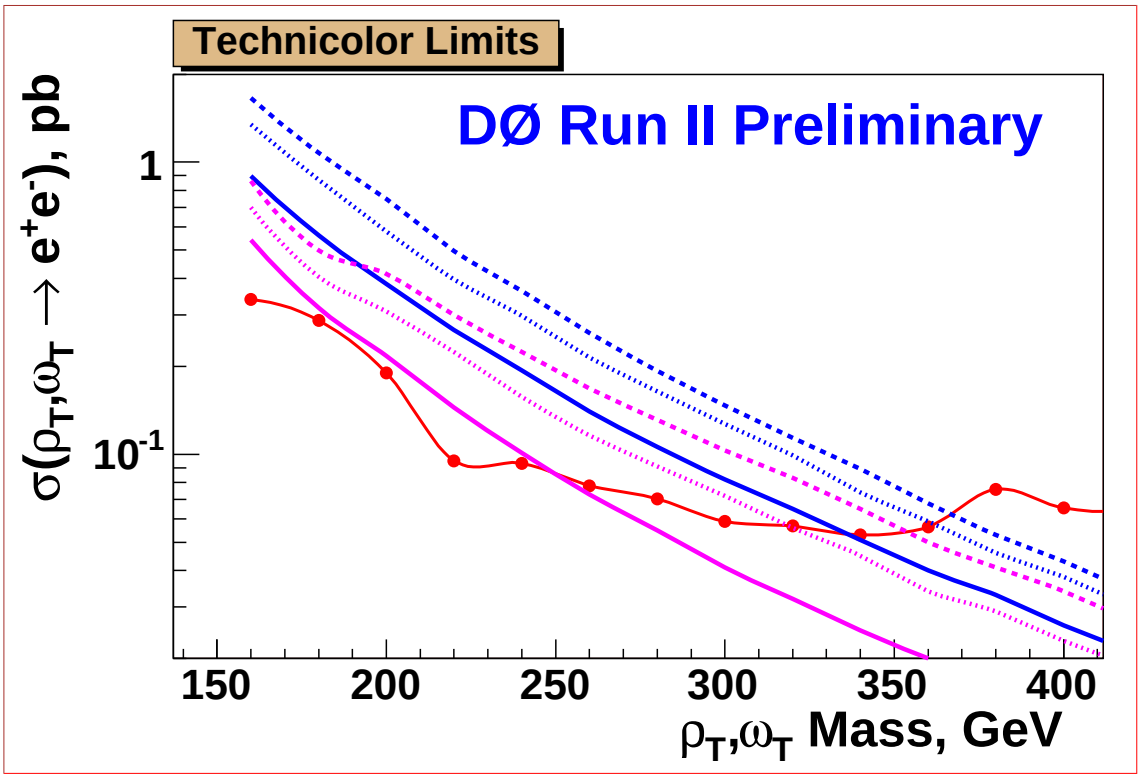

FIG. 2: Thick solid (black) curve: 95% CL upper bounds on the ρ_T, ω_T production cross section times its branching fraction into ee. The other curves show the cross section times branching fraction predicted by the technicolor model, for several values of the mass difference between ρ_T and The set of blue curves show the prediction for a mass difference $M(\rho_T) - M(\pi_T) = 60$ GeV (ie , while the set of magenta curves are for $M(\rho_T) - M(\pi_T) = 100$ GeV. The three curves for each set corresponds to values of M_V=500 GeV (uppermost), 200 GeV (middle) and 100 GeV (lowermost) respectively.

TABLE V: Upper 95% CL limits on $\rho_T, \omega_T \to ee$) as a function of the ρ_T, ω_T mass.

ρ_T, ω_T Mass	$\sigma^{95}(\rho_T, \omega_T \to ee)$
160 GeV	338 fb
180 GeV	287 fb
200 GeV	191 fb
220 GeV	95 fb
240 GeV	93 fb
260 GeV	78 fb
280 GeV	70 fb
300 GeV	59 fb
320 GeV	57 fb
340 GeV	53 fb
360 GeV	56 fb
380 GeV	76 fb
400 GeV	65 fb

The limit depends on the choice of the parameter M_V, also illustrated in Fig. 2. Here the experimental limit is compared to predictions in which the parameter M_V, which controls the ω_T cross section, is varied. For example, for values of $M_V > 100$ GeV we can rule out ρ_T and ω_T with masses below 340 GeV when mass difference between ρ_T and $\pi_T^{\pm}$ is smaller than the W mass. For a mass difference between ρ_T and $\pi_T^{\pm}$ of 100 GeV, we can rule out ρ_T and ω_T with masses below 250 GeV.

IV. CONCLUSIONS

We performed a search for techniparticles ρ_T and ω_T decaying into the dielectron channel using ~ 200 pb^{-1} of data collected by the DØ Experiment at the Fermilab Tevatron in 2002-2003 (Run II). The data are in excellent agreement with Drell-Yan production and do not exhibit any evidence for new physics beyond the Standard Model, so we use them to set limits on the existence of techniomega and technirho, predicted by recent technicolor models. For a mass difference between ρ_T and $\pi_T^{\pm}$ smaller than the mass of the W boson, the ρ_T and ω_T are ruled out at the 95% CL up to masses of 367 GeV. Limits obtained in this analysis are the most restrictive constraints on dilepton technicolor decays to date.

Acknowledgments

We thank Ken Lane and Stephen Mrenna for many helpful discussions regarding the details of their model and its implementation in Pythia MC. We thank the staffs at Fermilab and collaborating institutions, and acknowledge support from the Department of Energy and National Science Foundation (USA), Commissariat à l'Energie Atomique and CNRS/Institut National de Physique Nucléaire et de Physique des Particules (France), Ministry of Education and Science, Agency for Atomic Energy and RF President Grants Program (Russia), CAPES, CNPq, FAPERJ, FAPESP and FUNDUNESP (Brazil), Departments of Atomic Energy and Science and Technology (India), Colciencias (Colombia), CONACyT (Mexico), KRF (Korea), CONICET and UBACyT (Argentina), The Foundation for Fundamental Research on Matter (The Netherlands), PPARC (United Kingdom), Ministry of Education (Czech Republic), Natural Sciences and Engineering Research Council and WestGrid Project (Canada), BMBF (Germany), A.P. Sloan Foundation, Civilian Research and Development Foundation, Research Corporation, Texas Advanced Research Program, and the Alexander von Humboldt Foundation.

---

[1] DØ Collaboration, DØ Note 4349-Conf (2004), `http://www-d0.fnal.gov/Run2Physics/WWW/results/NP/NP02.pdf`.
[2] DØ Collaboration, DØ Note 4375-Conf (2004), `http://www-d0.fnal.gov/Run2Physics/WWW/results/NP/NP03.pdf`
[3] E. Eichten, K. Lane and J. Womersley, Phys. Lett. **B405**, 305-311 (1997).
[4] K. Lane, "Technihadron production and decay in low-scale technicolor", hep-ph/9903369.
[5] K. Lane, "Technihadron production and decay rates in the technicolor straw man model", hep-ph/9903372.
[6] K. Lane and S. Mrenna, "The Collider Phenomenology of Technihadrons in the Technicolor Strawman Model.", hep-ph/0210299, BUHEP-02-32, FERMILAB-PUB-02-267-T, Oct 2002, Phys. Rev. D **67**, 115011 (2003).
[7] CDF Collaboration, Phys. Rev. Lett. **84**, 1110 (2000).
[8] DØ Collaboration, DØ Note 4336-Conf, `http://www-d0.fnal.gov/Run2Physics/WWW/results/NP/NP01.pdf`.
[9] R. Hamberg, W.L. Van Neerven, and T. Matsura, Nucl. Phys. B**359**, 343 (1991); [Erratum-ibid. B**644**, 403 (2002)].
[10] H.L. Lai *et al.* (CTEQ Collaboration), Phys. Rev. **D51**, 4763 (1995).
[11] T. Sjostrand, P. Eden, C. Friberg, L. Lonnblad, G. Miu, S. Mrenna, and E. Norrbin, Comp. Phys. Comm. **135**, 238 (2001).
[12] H.L. Lai *et al.* (CTEQ Collaboration), Eur. Phys. J. C **12**, 375 (2000).
[13] I. Bertram *et al.* preprint Fermilab–TM–2104 (2000).